Optics Communications 321 (2014) 110–115

Contents lists available at ScienceDirect

Optics Communications

journal homepage: www.elsevier.com/locate/optcom

Confinement of ultracold atoms in a Laguerre–Gaussian laser beam created with diffractive optics

Sharon A. Kennedy, G.W. Biedermann, J.T. Farrar, T.G. Akin, S.P. Krzyzewski, E.R.I. Abraham*

Homer L. Dodge Department of Physics and Astronomy, University of Oklahoma, 440 W. Brooks St. Norman, OK 73019, USA

ARTICLE INFO

Article history:
Received 6 August 2013
Received in revised form
29 January 2014
Accepted 31 January 2014
Available online 11 February 2014

Keywords:
Laguerre–Gaussian mode
Toroid trap
Multiply-connected trap
Atom trap
Diffractive optics

ABSTRACT

We report 2D confinement of ^{87}Rb atoms in a Laguerre–Gaussian laser beam. Changing of the sign of the detuning from the atomic resonance dramatically alters the geometry of the confinement. With the laser detuned to the blue, the atoms are confined to the dark, central node of the Laguerre–Gaussian laser mode. This trapping method leads to low ac Stark shifts to the atomic levels. Alternatively, by detuning the laser to the red of the resonance, we confine atoms to the high intensity outer ring in a multiply-connected, toroidal configuration. We model the confined atoms to determine azimuthal intensity variations of the trapping laser, caused by slight misalignments of the Laguerre–Gaussian mode generating optics.

A laser propagating in the Laguerre–Gaussian (LG_p^ℓ) transverse mode is a versatile tool in atomic, molecular, and optical (AMO) physics. The $e^{i\ell\phi}$ azimuthal winding phase gives rise to an intrinsic quantized orbital angular momentum of $\ell\hbar$ per photon [1]. The additional quantum number may allow multi-dimensional quantum computing and encryption [2]. Experiments have been proposed [3] and demonstrated [4] that orbital angular momentum can be coupled from the optical field to the atomic internal states, revealed as a vortex state in a Bose–Einstein condensed (BEC) gas. The $p+1$ radial intensity nodes create cylindrically symmetric geometries, generating a manifold of multiply connected traps.

Blue-detuned dipole traps attract atoms to regions of low intensity, where the atoms scatter fewer photons and experience smaller ac Stark shifts. Cold atoms trapped in this configuration may be used in an atomic clock and other precision measurements. Dark optical traps have confined large numbers of atoms using an LG_0^3 beam [5], an arrangement of blue detuned lasers [6], and in other complex laser modes [7–12]. A dark toroidal geometry trap was created using a superposition of LG_p^ℓ beams [13]. A blue-detuned dipole trap generated from a spatial light modulator [14] and two crossed LG_p^ℓ laser modes generated from a spatial phase plate [15] trapped single atoms with long coherence times. For the LG_0^ℓ mode laser, the azimuthal winding phase ensures that the intensity necessarily goes to zero at the center of the laser beam, confining the atoms in the central region of the laser beam.

Alternatively, red-detuned dipole traps confine atoms in the high intensity region of the trapping laser. Degenerate gases excited into vortex states confined in toroidal geometry traps exhibit unique matter wave interference patterns [16]. Multiply connected traps locally pin vortices in BECs, making them ideal for ring shaped BEC rotational gyroscopes [17]. While it is possible to create a multiply connected trap using a magnetic trap whose center is plugged by a blue detuned fundamental mode laser [18], these traps are species and state selective. Optical traps circumvent this problem. For a red-detuned LG_0^1 mode laser, the atoms are confined in a toroidal geometry. A theoretical analysis has concluded that a BEC whose initial conditions are similar to those found in standard traps can be loaded into an LG_p^ℓ mode [19], and a theoretical calculation of the transition of a thermal gas to a BEC within the LG_p^ℓ laser mode itself has been done [20].

Diffractive optics can transform, external to the laser cavity, the Gaussian output of a laser into LG_p^ℓ modes. A diffractive optic is a transparent optic where lithography techniques are used to etch microscopic structures on the surface. These structures are designed such that the laser wavefront evolves into the desired form via Huygens' principle. Two optics are necessary to control both the intensity and the phase. Diffractive optics can create high-order LG_p^ℓ modes [21] with demonstrated mode purities much higher than those formed with other methods [22]. The compact diffractive optics have proven advantageous in quantum information processing, where the

* Corresponding author. Tel.: + 1 405 325 2961; fax: +1 405 325 7557.
E-mail addresses: abe@nhn.ou.edu, abraham@nhn.ou.edu (E.R.I. Abraham).

http://dx.doi.org/10.1016/j.optcom.2014.01.084
0030-4018

large numerical aperture of these optics gathers the largest fraction of the fluorescence emitted by an ion trapped on a chip [23–25]. Recently, diffractive optic elements have been used to create blue detuned bottle beam traps [26].

We report 2D confinement of ultracold ^{87}Rb atoms loaded from a magneto-optical trap (MOT) in both blue-detuned and red-detuned LG_0^1 (doughnut mode) laser beams. The atoms are confined to the central node of the LG_0^1 mode in the blue-detuned case, and the atoms are confined in the toroidal anti-node of the LG_0^1 for the red-detuned case. We align our LG_0^1 mode vertically (along the direction of gravity), maintaining cylindrical symmetry. The study of the atomic density distribution reveals asymmetries in the LG_0^1 mode. This provides an in situ measurement of the LG_p^ℓ mode purity and the possibility of more exotic confinement potentials.

Fig. 1 shows a schematic of the experiment. The trapping laser consists of a low-power external-cavity diode laser [27] amplified by an SDL tapered amplifier in the Master Oscillator Power Amplifier (MOPA) configuration locked at a frequency to the red of the $|^2S_{1/2}, F=2\rangle \rightarrow |^2P_{3/2}, F'=3\rangle$ cycling transition in ^{87}Rb using a Dichroic-Atomic-Vapor Laser Lock (DAVLL) [28]. A series of three cylindrical lenses shape and expand the elliptical 300 mW output of this laser to a symmetrical Gaussian profile with a $1/e^2$ beam radius of 12.5 mm. The beam is sent through two polarizing beam splitter cubes (PBC) to create three beams that are directed through the cell along the orthogonal axes and then retro-reflected. Three $\lambda/2$ retarding optics adjust the fraction transmitted and reflected by the PBCs, and thus the relative intensity of the three beams. Two of the beams are directed at 45° angles relative to the cell, while the third beam is directed along the axis of the anti-Helmholtz coils through the side of the cell.

A 10 mW external cavity diode laser repumps the atoms that fall into the $|F=1\rangle$ hyperfine level back into the cycling transition. After reshaping the output with an anamorphic prism pair and expanding the beam to a $1/e^2$ beam radius of 12.5 mm, we inject the repump laser through the back of one of the PBCs so that it is collinear with the trapping beam. This laser is tuned to the $|^2S_{1/2}, F=1\rangle \rightarrow |^2P_{3/2}, F'=2\rangle$ transition. Originally, this laser was locked on resonance using saturated absorption spectroscopy. However, we find it easier to use the saturated absorption spectrometer [27] to find the right transition, and lock the laser with a DAVLL. We then optimize the frequency of the repump laser by simply maximizing the number of trapped atoms in the MOT.

The vapor-cell MOT is created from a Rb vapor in a $1.4\times\ 1.4\times\ 11$ in the rectangular glass cell that offers large optical access. This cell is pumped with a Varian Turbo-V 250 ℓ/s vacuum pump roughed by a Varian DS 102 mechanical pump. A typical vacuum pressure is 10^{-8}–10^{-7} Torr. At the center of the trap a magnetic field gradient of 20 G/cm is created by supplying 13 A through two 20-turn, 11 cm diameter coils placed 8 cm apart in an anti-Helmholtz configuration. The MOT regularly produces $\sim 10^8$ atoms with temperatures between 0.1 and 20 mK depending on the degree to which background magnetic fields are canceled.

To optically confine the cold atom sample, we overlap a laser in the LG_p^ℓ mode with the MOT. The LG_p^ℓ modes have a radial electric field whose magnitude is proportional to the product of a Gaussian and an associated Laguerre polynomial $L_p^\ell(x)$, which gives the characteristic $p+1$ radial intensity nodes when $\ell > 0$. For a planar wave front propagating along the z-axis, the magnitude of the electric field at $z=0$ is given by the following:

$$u_p^\ell(r) = \sqrt{\frac{2P}{\pi w^2}}(-1)^p e^{-\imath\ell\phi} e^{-r^2/w^2} \left(\frac{\sqrt{2}r}{w}\right)^{|\ell|} L_p^\ell(2r^2/w^2), \tag{1}$$

where P is the laser power and w is the beam waist. The $e^{-\imath\ell\phi}$ term in Eq. (1) implies that there is a quantized azimuthal phase change

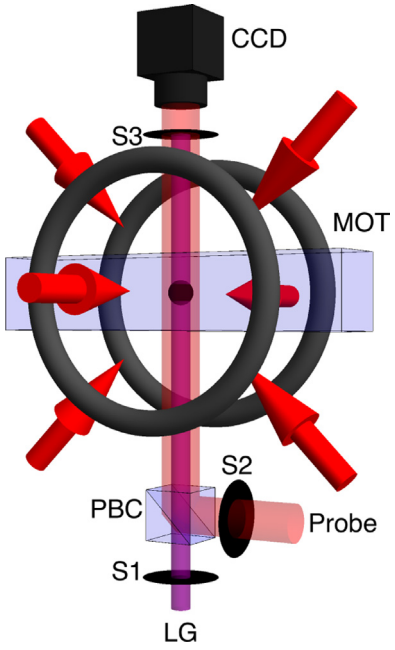

Fig. 1. This figure is a conceptional diagram of our experimental setup. Two of the MOT beams are directed at 45° relative to the cell. The third beam goes through the face of the cell along the axis of the magnetic field coils. The collinear probe and the LG_0^1 laser beams are directed vertically through the center of the MOT and are then sent into a CCD camera.

of $2\pi\ell$ in the electric field. This results in an intensity node at the center of the beam and an angular momentum of $\ell\hbar$ per photon. A Gaussian beam occurs when $\ell = p = 0$, whereas a donut beam occurs when $\ell > 0$ and $p=0$. As ℓ increases, so does the orbital angular momentum, and thus so does the effective size of the central node. This can be seen from Eq. (1), where the intensity has a functional form of $r^{2\ell}$ near $r=0$.

Cold atoms can be confined to either the nodes or the antinodes of these beams by means of the optical dipole force potential, which in the approximation of a two-level system and in the limit of the detuning being large compared to the natural linewidth, has the form:

$$U(r) = \frac{\hbar\Gamma^2}{4\Delta}\frac{I(r)}{I_{\text{sat}}}, \tag{2}$$

where $I(r)$ is the intensity distribution of the laser, I_{sat} is the saturation intensity, Δ is the detuning (the difference between the laser frequency and the transition frequency between the two states), and Γ is the linewidth of the excited atomic state. If the LG_p^ℓ laser is tuned above resonance (blue detuned, $\Delta > 0$), then the atoms will be repelled from regions of high intensity and confined to the nodes of the LG_p^ℓ laser mode, whereas if the laser is tuned below resonance (red detuned, $\Delta < 0$) then the atoms will be attracted to the anti-nodes.

The LG_0^1 laser beam is created using diffractive optics developed in collaboration with the research department of Diffractive Optics Corporation. These optics are advantageous in that they offer an external cavity method of creating very pure, higher-order LG_p^ℓ laser modes. Creating high-order LG_p^ℓ beams with computer generated holograms has a maximum mode purity of 80% intensity in the p mode of interest [29]. Our diffractive optics have demonstrated LG_p^ℓ beam creation with $>92\%$ of the output beam intensity in the desired mode [22]. We use two optics to generate the desired LG_p^ℓ beam, one to control the intensity, and the other to control the phase.

We spatially filter the 300 mW output of a second MOPA to obtain a more pure Gaussian beam. (Previously, for the highest

mode purity we used a single mode optical fiber to filter the beam.) The resulting 100 mW output of the spatial filter is telescoped to a $1/e^2$ beam radius of 0.5 mm and sent through the two LG_0^1 optics. We routinely get $\simeq 30$ mW of power in a pure LG_0^1 laser mode. The beam is then expanded by approximately a factor of four to increase the trapping volume. This results in a radial trap frequency of 30 Hz, at a detuning of 2 GHz. The beam is directed vertically through the center of the MOT.

A weak probe laser is resonant with the $|^2S_{1/2}, F=1\rangle \rightarrow |^2P_{3/2}F'=2\rangle$ transition, and propagates collinearly with the LG_0^1 beam. The probe beam is shuttered using a NEOS N23080 Acoustic Optical Modulator, and is used to image the cloud of atoms onto a Pulnix TM-300NIR CCD camera. Because the intensity of the LG_0^1 beam saturates our camera, a Uniblitz LS6T2 shutter is placed in the LG_0^1 beam path and a second shutter placed in front of the camera, so the LG_0^1 beam never enters the camera. First, the LG_0^1 shutter is closed. After 0.1 ms, the camera shutter is opened, and the probe is flashed 1.9 ms later. The shutter in front of the camera does not always fully open for shorter delays.

The cold atoms absorb the resonant light from the weak probe beam, and there is a reduction in intensity following Beer's law: $\ln(I_0/I_{\text{out}}) = \sigma_0 n$. Here, I_0 is the incident probe intensity, I_{out} is the probe intensity after passing through the atomic ensemble, σ_0 is the resonant photon scattering cross-section, and n is the integrated column density. In order to extract the atomic column density, we take a series of three CCD images. The probe beam is first imaged in the presence of the trapped atoms, measuring I_{out}. Then, I_0 is measured by imaging the probe absent any confined atoms. After blocking the probe laser, we expose the CCD chip and subtract this information (I_{bg}) from the previous two images. The column density at each CCD pixel is determined by the following:

$$n = \frac{1}{\sigma_0} \ln\left(\frac{I_0 - I_{\text{bg}}}{I_{\text{out}} - I_{\text{bg}}}\right). \tag{3}$$

The array of CCD pixels maps out the column density in a plane transverse to the direction of the probe beam propagation.

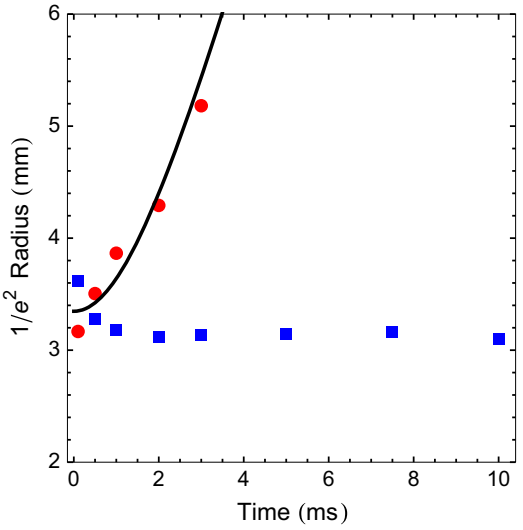

Fig. 2. The size of the atom cloud as a function of expansion time. The red circles represent the size of the atom cloud when there was no LG_0^1 beam present. The blue squares represent the size of the cloud with an LG_0^1 laser beam present detuned to the blue of the atomic resonance. With the LG_0^1 laser present, the size of the cloud remains approximately the same. This implies that the atoms are indeed confined to the center node of the LG_0^1 laser mode. Without the LG_0^1 laser beam present, in 4 ms the full cloud cannot be imaged nor a full $1/e^2$ radius be determined. The line is a fit to the expanding atoms with a fitted temperature of 20 mK. (For interpretation of the references to color in this figure caption, the reader is referred to the web version of this paper.)

We confine 10^7 ^{87}Rb atoms in the central node of an LG_0^1 laser beam detuned 2 GHz to the blue of the $|^2S_{1/2}, F=1\rangle \rightarrow |^2P_{3/2}\rangle$ resonance frequency. We first superimpose the LG_0^1 beam over the MOT. The repump laser is blocked, and the atoms are optically pumped into the $|F=1\rangle$ hyperfine level where they no longer interact with the MOT beams. The atoms are confined in 2D due to the repulsive force from the toroidal LG_0^1 beam surrounding the atoms. To detect the atoms we block the LG_0^1 beam and probe the remaining atoms with the absorption imaging procedure described above. We vary the delay between blocking the repump and probing the atoms. If the atoms are confined to the central node of the LG_0^1 beam, then the size of the atom cloud will not change with longer delays. If there is no confinement, then the atom cloud will expand at a rate related to its temperature.

The image from the CCD camera is fit to a Gaussian profile from which we can obtain the $1/e^2$ radius of the atom cloud. We find the density distribution is modeled accurately by a Gaussian. Fig. 2 shows the size of the atom cloud as a function of the delay between when the repump is blocked and the atoms are observed. The sizes of the atom cloud with and without the LG_0^1 beam are shown as blue squares and red circles respectively. When the LG_0^1 beam is superimposed over the MOT, the size of the atom cloud does not vary significantly as the delay time increased, indicating that the atoms are indeed confined to the central node of the LG_0^1 beam. When the LG_0^1 beam is not superimposed over the MOT, the atom cloud increases at a rate consistent with a temperature of 20 mK. The discrepancy in the cloud sizes between the two data sets at $t=0$ is consistent with run-to-run variations. It is also possible that the repulsive interactions of the blue-detuned LG_0^1 mode with the atoms at the edge of the MOT distort the initial distribution, making it larger than the MOT without the LG_0^1 beam.

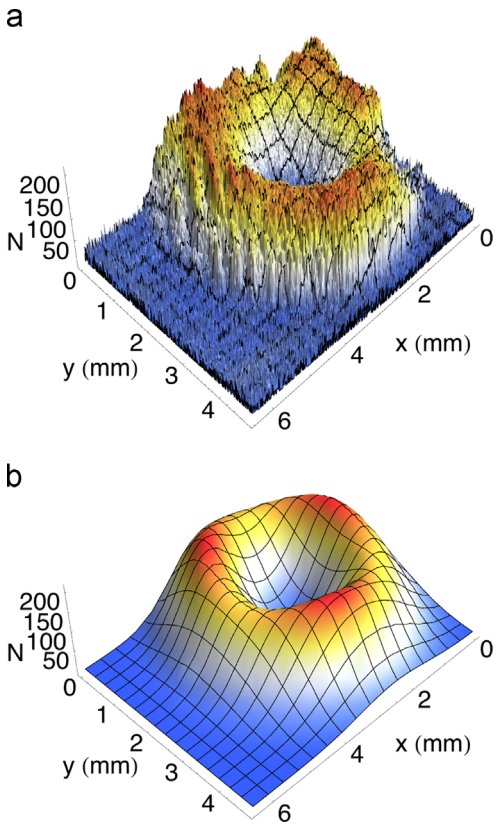

Fig. 3. (a) 3D CCD image of the number of atoms in the high-intensity region of our red-detuned LG $_0^1$ laser mode. In this image the Gaussian shaped profile of the atoms still confined in the MOT, but not confined in the high-intensity area has been removed. (b) Fit of Eq. (7) to the atom distribution in (a).

The initial decrease in the optically confined cloud size is due to the loss of those atoms from the MOT not confined by the LG_0^1 mode.

Fig. 3(a) shows an absorption image of 10^4 ultracold atoms trapped in a toroidal potential formed by a 30 mW LG_0^1 beam tuned 2 GHz to the red of the $|^2S_{1/2}, F=2\rangle \rightarrow |^2P_{3/2}\rangle$ transition. To perform this experiment we superimpose the LG_0^1 beam over the MOT, and image the atoms as described above. In this case, we do not turn off the MOT, so there are still atoms confined within the MOT that are not trapped in the LG_0^1 beam. We have subtracted these atoms from the absorption image to obtain Fig. 3(a).

The density distribution contained within the LG_0^1 is consistent with a Gaussian that is offset and rotated around the axis of symmetry. However, there is an azimuthal asymmetry in the density distribution, from variations in the intensity of the LG_0^1 laser beam due to misalignment of the diffractive optics [22]. This asymmetry in the intensity distribution manifests itself in the trap potential which causes a larger trap depth and more atoms in regions of higher intensity, shown in Figs. 3–5.

To model the system we assume the atoms obey Maxwell–Boltzmann statistics and the atomic density distribution is given by [30]:

$$n(r,\phi) = n_0 e^{-U(r,\phi)/k_B T}, \tag{4}$$

where n_0 is the peak density, k_B is the Maxwell–Boltzmann constant, T is the temperature, and $U(r,\phi)$ is the confining potential. The confining potential is given by Eq. (2), where $I(r) = |u_0^1(r)|^2$ for a pure LG_0^1 mode. Since the intensity of this mode is azimuthally symmetric, it does not fit our data. Tracing a path azimuthally around the absorption image, we note an oscillatory behavior in the atomic density distribution with a frequency of 3 Hz. We add a term to the model for the potential that oscillates with the same frequency. Our phenomenological model of the potential becomes

$$U_{\mathrm{LG}}(r,\phi) = -a\frac{2r^2}{w^2}e^{-r^2/w^2}(1+b\ \sin(3\phi+\phi_0)), \tag{5}$$

where b and ϕ_0 are fitting parameters that give the fractional size and location of the azimuthal asymmetries in the intensity profile. The parameter $a = \hbar\Gamma^2 I_0/4I_{\mathrm{sat}}\Delta k_B T$ is also a fitting parameter, where $I_0 = P/\pi w^2$ is the peak intensity of the trapping laser and P is the power of the trapping laser. To simplify our model, we approximate the potential as a simple harmonic oscillator. Expanding the potential to the second order about the equilibrium position $r = w/\sqrt{2}$, the potential becomes

$$U_{\mathrm{sho}}(r,\phi) = \left(\frac{4a}{ew^2}\left(r-\frac{w}{\sqrt{2}}\right)^2 - \frac{a}{e}\right)(1+b\ \sin(3\phi+\phi_0)) + \frac{a}{e}(1+b), \tag{6}$$

where the last term defines the zero of the potential to be at the minimum. Combining Eq. (6) with Eq. (4) gives the density

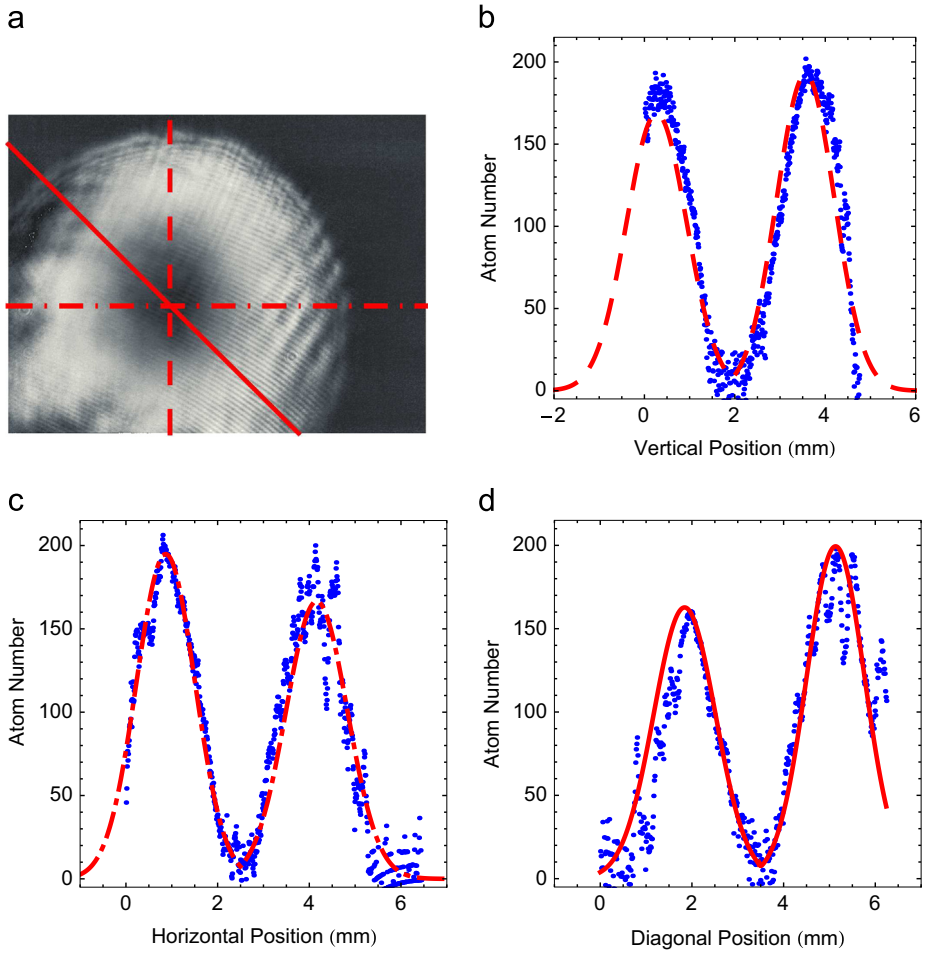

Fig. 4. (a) A 2D CCD image of the data shown in 3(a). Each cross section in (b)–(d) is indicated in the CCD image (a). The dashed red curve shows the vertical cross section, the dot-dashed red curve shows the horizontal cross section, and the solid red curve shows the diagonal cross section. The blue points are the data. For each cross section, ϕ is fixed and r is varied. (d) The largest azimuthal density difference. (For interpretation of the references to color in this figure caption, the reader is referred to the web version of this paper.)

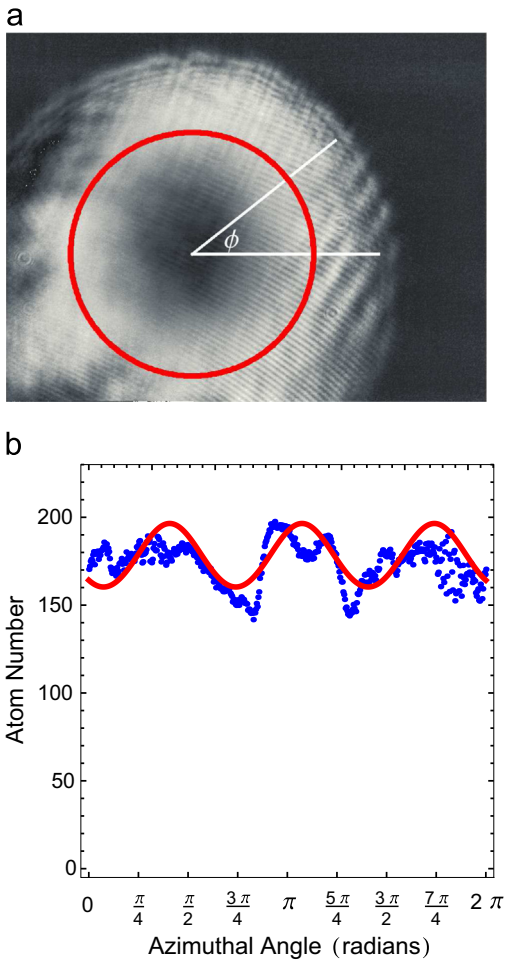

Fig. 5. (a) A 2D CCD image of the data shown in 3(a). The cross section is indicated in the CCD image by the solid red curve. (b) The blue points are the average of seven cross section separated by 40 μm, centered on the peak density. For each cross section, r is fixed and $0 \le \phi \le 2\pi$. The red curve is a fit of the data using Eq. (7), showing the $\sin 3\phi$ variations in the density. (For interpretation of the references to color in this figure caption, the reader is referred to the web version of this paper.)

distribution function:

$$n(r,\phi) = n_0 \exp\left\{-\left(\frac{4a}{ew^2}\left(r-\frac{w}{\sqrt{2}}\right)^2-\frac{a}{e}\right)(1+b\ \sin(3\phi+\phi_0))-\frac{a}{e}(1+b)\right\}. \quad (7)$$

Eq. (7) is fit to the data in Fig. 3(a), using *Mathematica*™, where a, b, w, and ϕ_0 are fitting parameters. Fig. 3(b) shows our best fit of our model for the density distribution. From the fit, we determine that the laser intensity varies by 13%. From our known laser power and the fitting results, we can also conclude that the temperature of the two-dimensionally confined atoms is 13 μK. This temperature is much less than the temperature of the MOT due to the shallow trap depth of the toroidal confining potential. Only the coldest fraction of the atoms from the MOT are confined. The measured temperature in the dipole trap is consistent with the theoretical trap depth of 10 μK calculated using the known power, detuning, and beam size.

Fig. 4(a) is a 2D CCD image of the data shown in Fig. 3(a). Each cross section for Fig. 4(b)–(d) is indicated in the CCD image, Fig. 4(a). Fig. 4(b)–(d) shows 1D cross sections of this data for fixed azimuthal angle ϕ. The blue points in each of the figures represent the absorption data along the cross section. The red dashed, dot-dashed, and solid lines are the theoretical fits from the model in Eq. (7). Fig. 4(d) shows the largest azimuthal density difference.

Sixty cross sections of the data in Fig. 3(a), in which the radial coordinate r is fixed but $0 \le \phi \le 2\pi$, were taken in 40 μm steps. Fig. 5(a) is the same as Fig. 4(a), where the cross section at the radial antinode is indicated. Fig. 5(b) shows an average of seven cross-sections centered at the peak density. The blue points represent the absorption data along the cross section. The red line is the theoretical fit from the model in Eq. (7). The $\sin 3\phi$ variation in density is clear in the data, and consistent with effects qualitatively observed in the intensity distribution of the LG_0^1 laser beam [22]. For cross sections interior and exterior to the peak density, the $\sin 3\phi$ azimuthal trend is difficult to resolve due to the noise in the data including large variations due to interference in the probe laser from multiple reflections.[1]

We successfully demonstrated 2D confinement of atoms from a MOT for both a blue-detuned LG_0^1 laser mode in which the atoms were confined in the center node of the laser beam and for a red detuned LG_0^1 laser mode in which the atoms were confined in the high-intensity ring. Asymmetries in the azimuthal intensity profile of the trapping laser appear as density inhomogeneities. From our model of the density distribution, we determined that the confining potential fluctuates by 13% along the azimuthal direction. We did not make any attempt to optimize azimuthal symmetry in this study. From previous work [22], these variations can be eliminated with better alignment through the diffractive optics. However, this work also indicates that a systematic study of the purposeful misalignment of the diffractive optics in warranted to create new confinement potentials such as ferris wheel traps [32].

High purity (symmetric) LG_p^ℓ modes are important for degenerate gas applications, gyroscopes, and vortex matter-wave creation, stability, and interferometry. We have shown that analysis of the atomic distribution is a method to analyze the symmetry of the LG_p^ℓ transverse mode in situ for systems where regular analysis of the full, high-intensity trapping beam is not feasible. Also, purposeful creation of periodic, azimuthal intensity variations in the LG_p^ℓ modes may provide multiple traps for the toroidal geometries, increasing the range of experiments accessible to LG_p^ℓ beams made by diffractive optics.

Acknowledgments

This work was supported by The Research Corporation, Digital Optics Corporation, and the University of Oklahoma.

References

[1] L. Allen, M.W. Beijersbergen, R.J.C. Spreeuw, J.P. Woerdman, Phys. Rev. A 45 (1992) 8185, http://dx.doi.org/10.1103/PhysRevA.45.8185.
[2] G. Molina-Terriza, J.P. Torres, L. Torner, Nat. Phys. 3 (2007) 305.
[3] K.-P. Marzlin, W. Zhang, E.M. Wright, Phys. Rev. Lett. 79 (24) (1997) 4728, http://dx.doi.org/10.1103/PhysRevLett.79.4728.
[4] K.C. Wright, L.S. Leslie, N.P. Bigelow, Phys. Rev. A 77 (4) (2008) 041601, http://dx.doi.org/10.1103/PhysRevA.77.041601.
[5] T. Kuga, Y. Torii, N. Shiokawa, T. Hirano, Y. Shimizu, H. Sasada, Phys. Rev. Lett. 78 (1997) 4713, http://dx.doi.org/10.1103/PhysRevLett.78.4713.
[6] N. Davidson, H. Jin Lee, C.S. Adams, M. Kasevich, S. Chu, Phys. Rev. Lett. 74 (1995) 1311, http://dx.doi.org/10.1103/PhysRevLett.74.1311.
[7] J.L. Chaloupka, Y. Fisher, T.J. Kessler, D.D. Meyerhofer, Opt. Lett. 22 (13) (1997) 1021, http://dx.doi.org/10.1364/OL.22.001021.
[8] R. Ozeri, L. Khaykovich, N. Davidson, Phys. Rev. A 59 (1999) R1750, http://dx.doi.org/10.1103/PhysRevA.59.R1750.
[9] R. Ozeri, L. Khaykovich, N. Davidson, Phys. Rev. A 65 (2002) 069903, http://dx.doi.org/10.1103/PhysRevA.65.069903.

[1] A *Mathematica*™ notebook containing the data and all 60 cross-sections can be found online at [31].

[10] R. Ozeri, L. Khaykovich, N. Friedman, N. Davidson, J. Opt. Soc. Am. B 17 (7) (2000) 1113, http://dx.doi.org/10.1364/JOSAB.17.001113.
[11] S. Kulin, S. Aubin, S. Christe, B. Peker, S.L. Rolston, L.A. Orozco, J. Opt. B: Quantum Semiclass. Opt. 3 (6) (2001) 353.
[12] L. Isenhower, W. Williams, A. Dally, M. Saffman, Opt. Lett. 34 (8) (2009) 1159, http://dx.doi.org/10.1364/OL.34.001159.
[13] S.E. Olson, M.L. Terraciano, M. Bashkansky, F.K. Fatemi, Phys. Rev. A 76 (2007) 061404, http://dx.doi.org/10.1103/PhysRevA.76.061404.
[14] P. Xu, X. He, J. Wang, M. Zhan, Opt. Lett. 35 (13) (2010) 2164, http://dx.doi.org/10.1364/OL.35.002164.
[15] G. Li, S. Zhang, L. Isenhower, K. Maller, M. Saffman, Opt. Lett. 37 (5) (2012) 851, http://dx.doi.org/10.1364/OL.37.000851.
[16] J. Tempere, J.T. Devreese, E.R.I. Abraham, Phys. Rev. A 64 (2001) 023603, http://dx.doi.org/10.1103/PhysRevA.64.023603.
[17] S. Thanvanthri, K.T. Kapale, J.P. Dowling, J. Mod. Opt. 59 (13) (2012) 1180, http://dx.doi.org/10.1080/09500340.2012.702228.
[18] C. Ryu, M.F. Andersen, P. Cladé, V. Natarajan, K. Helmerson, W.D. Phillips, Phys. Rev. Lett. 99 (2007) 260401, http://dx.doi.org/10.1103/PhysRevLett.99.260401.
[19] E.M. Wright, J. Arlt, K. Dholakia, Phys. Rev. A 63 (1) (2000) 013608, http://dx.doi.org/10.1103/PhysRevA.63.013608.
[20] T.G. Akin, S. Kennedy, B. Dribus, J.L. Marzuola, L. Johnson, J. Alexander, E.R. I. Abraham, Opt. Commun. 285 (1) (2012) 84, http://dx.doi.org/10.1016/j.optcom.2011.09.011.
[21] S. Khonina, V. Kotlyar, R. Skidanov, V. Soifer, P. Laakkonen, J. Turunen, Opt. Commun. 175 (4–6) (2000) 301, http://dx.doi.org/10.1016/S0030-4018(00)00472-7.
[22] S.A. Kennedy, M.J. Szabo, H. Teslow, J.Z. Porterfield, E.R.I. Abraham, Phys. Rev. A 66 (2002) 043801, http://dx.doi.org/10.1103/PhysRevA.66.043801.
[23] E.W. Streed, B.G. Norton, A. Jechow, T.J. Weinhold, D. Kielpinski, Phys. Rev. Lett. 106 (2011) 010502, http://dx.doi.org/10.1103/PhysRevLett.106.010502.
[24] T. Kim, P. Maunz, J. Kim, Phys. Rev. A 84 (2011) 063423, http://dx.doi.org/10.1103/PhysRevA.84.063423.
[25] G. Brady, A. Ellis, D. Moehring, D. Stick, C. Highstrete, K. Fortier, M. Blain, R. Haltli, A. Cruz-Cabrera, R. B riggs, J. Wendt, T. Carter, S. Samora, S. Kemme, Appl. Phys. B 103 (4) (2011) 801.
[26] V.V. Ivanov, J.A. Isaacs, M. Saffman, S. Kemme, A. Ellis, G. Brady, J. Wendt, G.W. Biedermann, S. Samora, Atom trapping in a bottle beam created by a diffractive optical element, arxiv:1305.5309[physics.atom-ph].
[27] K.B. MacAdam, A. Steinbach, C. Wieman, Am. J. Phys. 60 (12) (1992) 1098, http://dx.doi.org/10.1119/1.16955.
[28] A. Millett-Sikking, I.G. Hughes, P. Tierney, S.L. Cornish, J. Phys. B: At. Mol. Opt. Phys.: At. 40 (1) (2007) 187.
[29] J. Arlt, K. Dholakia, L. Allen, M.J. Padgett, J. Mod. Opt. 45 (6) (1998) 1231, http://dx.doi.org/10.1080/09500349808230913.
[30] R. Grimm, M. Weidemüller, Y.B. Ovchinnikov, Adv. At. Mol. Opt. Phys. 42 (2000), 95–170. http://dx.doi.org/10.1016/S1049-250X(08)60186-X (Academic Press).
[31] T.G. Akin, E.R.I. Abraham, Mathematica™ calculation. ⟨http://nhn.nhn.ou.edu/~abe/research/lgbeams/index.html⟩, 2013.
[32] S. Franke-Arnold, J. Leach, M.J. Padgett, V.E. Lembessis, D. Ellinas, A.J. Wright, J. M. Girkin, P. Ohberg, A.S. Arnold, Opt. Express 15 (14) (2007) 8619, http://dx.doi.org/10.1364/OE.15.008619.